THE ASTROPHYSICAL JOURNAL, 255: 128–142, 1982 April 1

H_2O MASERS IN W49N. I. MAPS

R. C. WALKER
National Radio Astronomy Observatory,[1] Charlottesville, Virginia
D. N. MATSAKIS
University of California, Berkeley
AND
J. A. GARCIA-BARRETO
Research Laboratory of Electronics, Massachusetts Institute of Technology
Received 1981 May 15; accepted 1981 October 6

ABSTRACT

A multiple point fringe rate map of H_2O masers in W49N is presented that shows the locations of 386 separate features. The principal results, readily apparent in the map, are the clear separation of positive and negative high-velocity features and the presence of isolated features outside the centers of activity noted in earlier observations. The distribution of features suggests that the masers are seen in regions where material, which has been accelerated near a central star to velocities of up to a few hundred km s^{-1}, is interacting with a surrounding stationary or slowly moving medium.

Subject headings: interstellar: molecules — masers — nebulae: individual — radio sources: identifications — stars: formation

I. INTRODUCTION

The H II region, W49N, probably contains the most complex H_2O maser source in the Galaxy. Total power spectra show that it contains hundreds of features spread over more than 500 km s^{-1}. This complexity makes it an attractive object to study with high spatial resolution. It might allow patterns in the distribution of features to be discerned that would not be apparent in simpler sources and which might help clarify the nature of H_2O maser emission regions.

Previous VLBI observations of H_2O in W49N showed a close association between high- and low-velocity features and gave a suggestion that the positive and negative high-velocity features were well separated (Knowles *et al.* 1974; Walker *et al.* 1977; Genzel *et al.* 1978). The features seemed to be grouped into several centers of activity, all of which contained low-velocity features and several of which contained high-velocity features. Within a given center, the high-velocity features were more dispersed than the low-velocity features. These centers could be interpreted as separate protostars, each with its surrounding envelope in which the conditions for maser emission are favorable. The apparent separation of positive and negative high-velocity features suggested that the various centers were not entirely isolated but that some global phenomenon was influencing flows throughout the region.

In an effort to define the centers of activity more thoroughly and to check on the separation of the positive and negative high-velocity features, we have observed the source with considerably improved sensitivity compared to previous observations. A multiple point fringe rate mapping technique has been applied to the data that allows several features to be mapped at each velocity. The resulting map contains 386 separate maser features. The separation of the positive and negative high velocity features is confirmed with much improved statistics. However, while many features are found in clusters, there are a significant number of isolated features. These isolated features, which have both high and low velocities, are seen at distances of 10^{17} cm and more from the nearest center of activity. The implications of the distribution of features for the geometry of the maser region are discussed in § IV. Later papers in this series will present more detailed analyses of the map including a statistical demonstration of the presence of hyperfine structure, a study of clustering scale sizes and velocity gradients using two-point correlation functions, and an attempt to relate the statistical properties of the map with possible geometries and physical conditions in the source.

II. THE OBSERVATIONS

The H_2O masers in W49N, W3(OH), and W3–IRS 5 were observed on 1978 June 14–16 with the three-element interferometer consisting of the Haystack 37 m, the National Radio Astronomy Observatory 43 m, and the Owens Valley Radio Observatory 40 m telescopes. Maser receivers and maser frequency standards were used at all sites. In order to cover the wide velocity range in W49N, the local oscillators were switched over two or four frequencies with 1 s spent at each frequency during each cycle. The source was observed for three days using two sets of four frequencies on each of 2 days and a single set of two frequencies on a third day. Every set of

[1] The National Radio Astronomy Observatory is operated by Associated Universities, Inc. under contract to the National Science Foundation.

frequencies included one band centered on 17.1 km s^{-1} in which a reference feature was found. A total of 14 different 2 MHz windows were observed in this manner. The data were recorded with a 2 MHz bandwidth and processed on the NRAO Mark II VLBI processor (Clark 1973) with a velocity resolution of about 0.2 km s^{-1}. The results of the W3–IRS 5 and W3(OH) observations are presented in Walker (1981).

The interferometer fringe phases were calibrated using a reference channel at 11.6 km s^{-1}. While none of the channels in the reference band had constant visibility amplitudes as would be produced by an ideal, point source phase reference, the channel at 11.6 km s^{-1} did not have the large, rapid variations in amplitude seen in most of the others. It did have a high frequency ripple indicating the presence of two, well separated features, one with about 30% of the flux density of the other. It also had low but nearly constant amplitudes, other than the ripple, on the long baselines indicating that the features were up to 80% resolved and had simple structures. The effects of the beating of the two features were reduced by using a running average phase as the phase reference. The beating did not cause significant problems in the map as indicated by the lack of ghost images of other strong features. The resolution of the reference feature may cause uncertainties in the positions of features in the map, but those uncertainties should be reflected in the formal errors from the least-squares solutions used to find positions. Fluctuations in the reference phase could limit the dynamic range of the fringe rate spectra and, therefore, of the map. While the magnitude of this effect is not well understood for this experiment, it is probably not significantly greater than limits imposed by noise, confusion, and uncertainties in the amplitude calibration.

The amplitudes were calibrated using the total power spectra of the recorded data from each antenna following the method described by Reid *et al.* (1980), and using an empirically determined factor of 2.0 to correct for local oscillator problems at Owens Valley. The method ensures the consistent calibration as a function of time and baseline that is required for mapping. However, the relative scaling of the various frequency windows and the absolute scaling in terms of flux density depend on system temperature measurements, antenna calibration, and comparison of lines in the overlapping regions of the windows. The uncertainties in these measurements, for this experiment, leave the absolute flux scale uncertain by a factor on the order of 30%. Any differences in measured flux density between our data and other published data should be treated with caution.

The maps were made using the multiple point fringe rate method originally described by Giuffrida (1977) and developed to its current form for the reduction of this experiment. The method is described in detail by Walker (1981). Aperture synthesis or phase fitting techniques were not used due to the difficulty of calibrating phase slopes introduced by clock errors. Unlike the single point fringe rate method used in the previous observations of W49N, the multiple point method allows several features to be mapped at each velocity. The method does assume each feature is a point source, but this assumption is probably not too bad as shown by the aperture synthesis results of Walker *et al.* (1978), Reid *et al.* (1980), and Genzel *et al.* (1981) for astrophysical masers. For a partially resolved feature, the method will find less than the total flux density and will give a position that, depending on size and degree of symmetry, may be more poorly determined than if the feature were a point source. In cases of extreme confusion, such as obviously exists in the low velocity region of W49N, only the few strongest features at each velocity will be mapped. As with any VLBI observations, large, smooth features will not be seen.

Two limitations of the method required extra care in map making. Features well separated from the phase center of a map have fringe rates that change rapidly with time. This can lead to smeared fringe rate peaks, and it also limits the field of view of each map (see Walker 1981). In the case of W49N, fields of view 0.″5 in R.A. and 2.″0 in decl. were used in order to avoid this problem. The other problem is the tendency of the map making program to find spurious features when there are several closely spaced features. The method is based on the fact that each peak in a fringe rate spectrum confines the corresponding feature to lie on a line on the sky. An effort was made to avoid spurious features by carefully examining plots of such lines and checking the reality of each of the sets of intersections that the program thought was a feature. We feel that, as a result of the care taken, there are very few, if any, spurious features on the map. This does not mean that the map is complete as will become obvious in the discussion below.

III. RESULTS

The map of W49N contains 386 features separated by up to 4.″0 with typical relative position error bars of 0.″001 in R.A. and 0.″003 in decl. This presents a serious display problem which we attempt to resolve by first showing the full map in Figure 1 and then showing expanded views of the more interesting regions in succeeding figures. In each map, the area of the circle representing a feature is proportional to the flux density of the feature. The position error bars are also shown in the small scale maps. On each map, the velocities of features which do not appear on a smaller scale map are shown. For each feature, the velocity, flux density, and right ascension and declination offsets from the reference position, with their one sigma errors, and the total velocity range over which the feature was detected are presented in Table 1. The total velocity range, rather than the line width, is given because of difficulties in determining the latter quantity for the many features which are asymmetric or were only detected on one side of the peak.

Figure 2 shows the total power spectrum of W49N at the time of the observations. It also shows the sum of the flux densities in the map points at each velocity. It is clear that, while all of the flux density is accounted for in a few portions of the spectrum, a large fraction of the total flux density is not accounted for. This is due to a combination of two effects, both of which reduce the flux density seen in

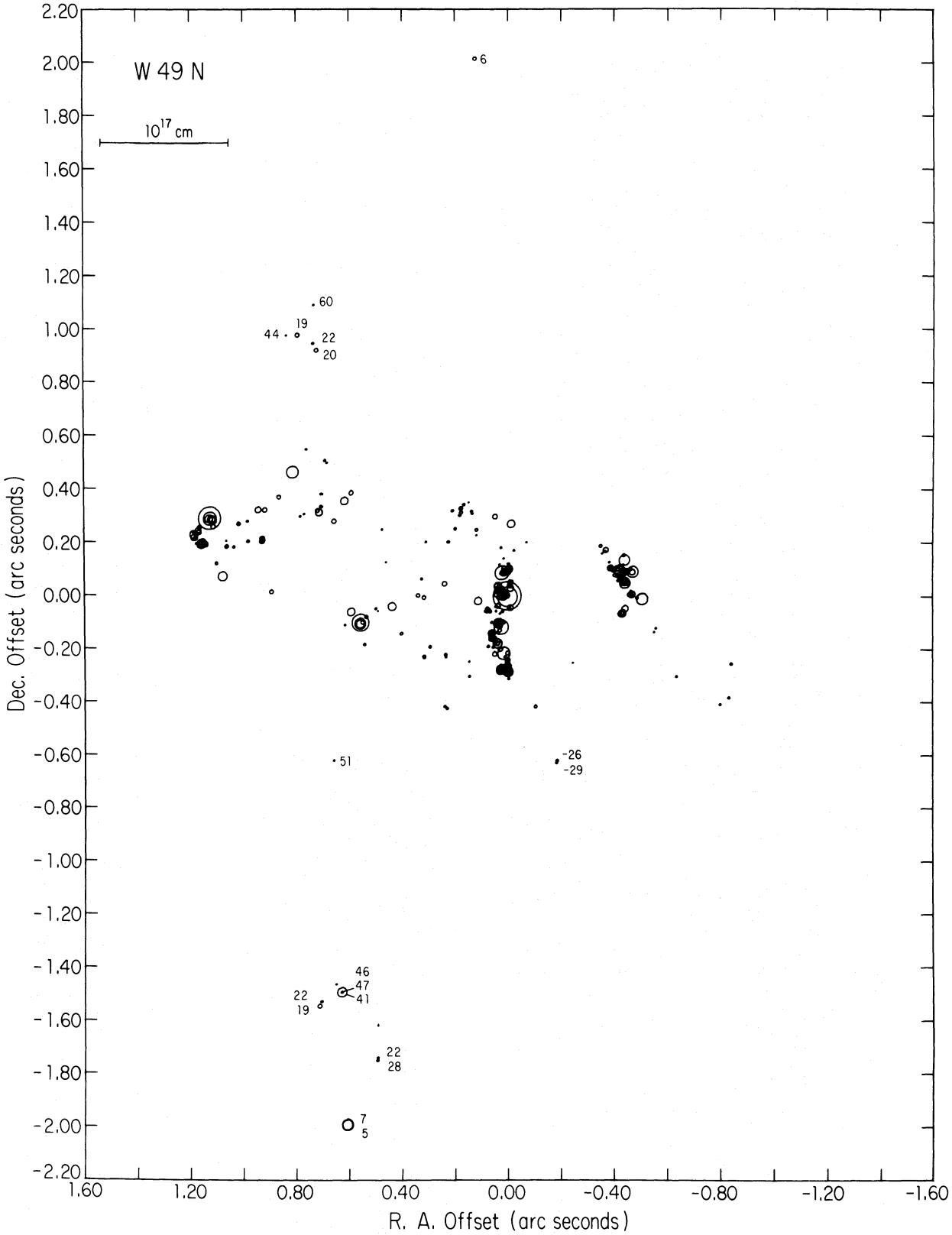

FIG. 1.—Map of H_2O masers in W49N. The area of each symbol is proportional to the flux density of the feature. The velocity, in km s^{-1}, of each feature that is not shown in smaller scale maps is written by the feature. The scales shown by the bars in all maps assume a distance of 14 kpc to W49N (Wilson 1975).

TABLE 1

WATER MASERS IN W49N

VELOCITY KM S^{-1}	FLUX JY	RA OFFSET 0".001		DEC OFFSET 0".001		RANGE KM S^{-1}
-219.8	21	-557.8	+-1.6	-119.4	+-1.7	1.7
-217.3	14	-551.3	7.2	-134.6	4.0	0.6
-217.2	19	39.2	0.5	-133.9	2.5	1.9
-214.7	125	25.0	0.1	-102.5	0.5	2.7
-212.4	370	35.8	0.1	-98.0	0.5	2.5
-210.4	811	35.2	0.1	-99.3	0.3	2.1
-208.9	382	35.8	0.1	-98.7	0.4	1.3
-207.7	387	35.9	0.1	-98.6	0.3	4.2
-203.8	43	-840.7	0.6	-255.4	1.9	2.3
-201.7	27	36.3	0.2	-98.8	0.9	3.6
-196.0	25	-404.6	1.6	96.1	3.2	1.5
-192.5	27	-799.4	1.6	-408.3	2.8	1.1
-183.0	39	-832.3	0.6	-383.6	5.0	1.9
-182.9	68	-388.5	0.4	104.0	1.5	1.1
-182.1	86	-389.1	0.5	103.7	2.5	1.1
-179.3	302	-386.0	2.5	107.3	2.8	4.0
-176.6	80	-387.7	1.5	106.0	4.0	2.7
-174.0	72	34.3	0.2	-105.6	0.8	1.5
-172.4	27	-410.6	2.9	83.0	5.7	2.1
-168.5	22	-396.3	5.4	94.7	8.0	3.6
-166.0	13	-408.8	8.1	78.6	11.7	1.9
-163.1	19	-398.6	11.4	105.8	20.6	2.3
-162.5	13	39.2	0.8	-136.3	0.9	2.1
-161.8	25	-381.6	5.4	129.0	15.4	0.6
-161.1	75	-412.6	0.4	77.5	1.0	1.1
-160.0	80	-402.4	1.4	80.4	2.6	1.1
-159.5	92	-460.4	0.4	102.0	1.5	1.9
-157.6	35	-414.7	1.2	59.0	4.2	1.5
-153.4	174	-433.9	1.4	79.5	2.7	4.0
-152.8	53	-457.6	0.4	4.5	1.3	0.6
-152.1	50	-458.0	0.2	6.5	1.3	1.1
-151.2	27	-418.8	0.9	65.8	6.2	0.6
-150.0	112	-457.6	1.1	7.5	2.5	2.3
-149.3	63	-419.8	0.6	83.8	2.6	1.1
-149.0	37	-458.6	2.3	11.6	10.5	1.9
-147.0	15	31.5	0.6	120.2	3.3	1.9
-146.3	60	-460.8	0.8	10.9	1.2	1.3
-144.4	24	-432.7	3.1	80.3	12.5	1.5
-144.0	9	26.4	0.6	-167.8	6.8	1.1
-142.8	94	-459.1	1.6	7.3	4.5	1.5
-141.9	10	-245.5	1.1	-248.1	7.8	1.1
-141.1	85	-433.0	0.3	78.5	4.2	1.7
-140.2	27	-635.5	0.8	-302.7	1.8	1.3
-139.1	23	-463.3	1.8	20.0	6.0	0.8
-137.5	12	25.3	0.5	-276.2	2.0	1.1
-136.1	158	-430.5	0.8	81.2	1.1	3.2
-135.3	267	24.8	0.1	-274.1	0.4	1.5
-134.5	133	546.9	1.0	-96.4	3.0	0.8
-133.3	858	24.6	0.1	-274.1	0.4	2.3
-131.8	404	24.2	0.1	-274.4	0.3	1.3
-130.6	48	24.7	0.2	-275.1	0.7	1.3
-129.8	66	-451.7	3.0	89.3	3.6	1.7
-129.5	16	24.8	1.2	-272.6	1.6	1.1
-128.2	73	-464.8	0.6	8.0	2.5	1.5
-127.8	38	20.6	0.5	-267.4	1.6	1.3
-127.5	94	72.0	0.4	-48.7	0.8	1.5
-127.0	48	23.8	0.4	-273.3	1.4	1.3
-126.9	93	77.2	0.2	-44.8	0.9	1.3
-125.6	67	73.0	0.1	-49.1	0.7	0.9
-125.3	397	-467.0	0.1	7.8	0.4	2.3
-123.6	87	-466.0	1.3	1.6	7.7	0.8
-123.4	18	27.1	3.8	-283.1	5.8	0.5
-122.6	1005	-438.4	0.6	136.2	0.9	3.2
-119.9	58	30.4	0.2	-274.9	0.8	3.6
-119.8	45	-427.7	4.7	98.8	6.1	0.8
-118.9	83	533.6	+-0.3	-76.8	+-1.2	1.9
-118.3	44	72.7	0.4	-49.9	0.8	1.1
-117.8	80	-408.0	1.2	108.7	3.4	1.5
-117.7	17	26.6	0.4	-269.8	2.1	0.8
-115.4	69	-436.7	0.7	154.5	2.2	2.3
-114.2	55	-432.4	2.3	117.1	5.5	0.6
-113.2	470	111.6	0.1	-16.4	0.3	1.9
-111.4	179	21.2	0.1	88.2	0.3	2.1
-110.4	273	-469.5	0.3	90.9	1.3	0.8
-109.4	1703	21.3	0.0	89.4	0.4	3.0
-108.3	15	-355.4	2.8	160.9	8.6	0.2
-107.1	40	83.7	0.3	-54.6	1.5	1.5
-106.8	22	19.6	2.3	105.2	13.7	1.1
-106.6	14	20.2	1.0	90.4	4.3	0.4
-105.6	259	-432.7	0.4	98.1	1.3	3.4
-104.3	14	15.9	0.7	142.6	2.7	0.8
-104.2	11	146.2	0.4	-244.4	2.1	0.6
-104.0	66	-348.9	0.4	188.9	1.5	1.5
-102.8	99	79.8	0.4	-53.6	1.1	0.6
-102.6	399	29.2	0.2	-278.9	0.6	2.3
-101.8	1091	-470.4	0.2	92.2	1.0	2.9
-98.9	10	68.7	0.5	-151.6	2.1	0.8
-98.1	32	-365.7	0.4	168.9	1.7	0.2
-97.8	151	-446.0	0.5	58.1	2.5	2.2
-96.3	233	-368.5	0.8	174.0	6.0	0.6
-95.5	551	436.8	0.2	-37.5	0.9	0.6
-95.2	359	14.0	0.1	88.4	1.1	3.8
-94.5	192	-436.9	1.3	49.6	3.6	3.0
-93.4	47	198.8	0.5	253.0	2.5	1.3
-93.2	24	25.3	0.3	181.9	2.2	1.9
-92.8	53	-486.9	0.4	-5.0	4.3	0.6
-92.0	12	198.4	0.6	254.8	1.7	1.3
-91.0	101	339.0	0.8	4.1	3.8	1.5
-89.0	167	-470.1	0.4	11.0	1.2	1.7
-89.0	17	2.9	1.4	100.8	2.7	1.5
-87.0	123	-444.6	0.8	59.7	1.8	2.1
-85.8	106	316.6	0.7	-3.6	5.6	1.7
-85.6	154	-445.1	0.8	57.3	1.6	2.1
-83.8	18	210.7	0.3	321.1	1.8	0.9
-83.4	21	-9.4	0.5	-44.0	2.9	1.7
-83.3	35	1.9	0.2	92.2	0.9	2.3
-83.1	20	48.8	1.3	-180.4	3.8	1.1
-82.4	125	-445.8	1.4	91.9	2.0	2.1
-82.1	52	210.3	0.5	319.9	2.4	1.9
-81.3	360	-441.6	1.0	-45.4	6.8	1.5
-80.9	50	73.0	0.3	-187.3	0.9	1.5
-80.8	117	178.3	1.1	328.9	2.2	2.3
-79.3	359	-447.0	0.3	92.3	1.7	2.1
-79.3	78	177.1	0.6	313.1	2.4	0.8
-78.8	65	2.7	0.9	94.2	2.1	0.6
-78.7	56	182.0	1.3	303.0	6.2	0.8
-78.5	506	-431.0	0.7	-62.6	2.3	2.1
-77.6	96	1.0	0.7	93.2	0.8	1.9
-77.4	32	178.3	0.3	324.8	2.1	1.3
-76.0	481	-430.9	0.2	-63.1	2.4	1.9
-75.7	144	1.1	0.5	93.8	1.0	1.3
-75.0	125	63.2	0.7	-148.2	1.3	1.3
-74.9	363	0.5	0.1	93.2	0.3	2.5
-73.7	135	-0.2	0.4	-248.9	1.6	1.7
-72.3	122	0.5	0.1	93.5	1.0	0.6
-71.7	67	0.9	0.2	91.0	1.5	1.5
-71.6	264	-427.4	1.0	-64.2	1.2	2.1
-70.2	149	42.7	0.2	7.9	0.4	3.0
-69.3	70	2.1	0.5	-253.8	1.3	1.5
-67.6	16	44.2	1.0	-53.7	5.3	1.1

TABLE 1—*Continued*

VELOCITY KM S^{-1}	FLUX JY	RA OFFSET 0^m.001		DEC OFFSET 0^m.001		RANGE KM S^{-1}
-67.4	7	179.2	+-1.1	330.7	+-3.4	0.4
-66.8	13	55.2	0.4	-143.3	1.3	0.4
-66.5	13	35.8	3.0	7.6	8.9	1.1
-64.4	76	3.3	0.1	105.7	0.3	1.9
-63.8	106	-423.4	0.9	-67.6	3.9	1.1
-63.6	18	-3.4	0.9	84.8	3.4	0.4
-63.4	28	-4.5	0.3	-251.3	1.6	1.5
-62.4	979	-441.0	0.2	50.6	0.5	4.0
-61.3	38	9.0	1.4	-226.3	4.5	0.9
-60.6	29	38.9	0.2	-38.1	0.8	1.7
-60.5	73	-420.5	0.4	-63.8	7.7	1.1
-59.6	22	233.2	1.2	-226.8	3.1	0.8
-58.8	228	-442.4	0.5	52.2	2.2	3.4
-58.7	49	234.4	0.6	-217.4	0.9	1.3
-58.3	39	137.9	0.2	318.8	0.7	1.3
-58.3	32	5.4	1.3	-243.5	5.5	1.3
-56.3	36	31.3	0.5	39.5	1.9	0.8
-56.1	34	-439.0	1.1	54.7	5.0	0.8
-56.1	21	181.6	0.6	330.0	2.4	1.7
-55.6	56	-3.0	0.3	102.5	2.9	2.1
-55.5	29	-440.4	0.6	55.9	2.7	1.1
-55.4	16	2.4	1.5	-263.7	1.5	0.6
-54.9	63	-1.3	0.4	106.1	0.8	1.7
-54.5	32	54.1	0.8	-159.5	3.0	0.4
-54.5	39	6.7	0.7	-262.0	2.5	1.5
-53.3	49	4.3	0.6	-237.0	5.0	0.4
-52.9	274	52.5	0.8	-157.9	1.6	2.5
-52.6	258	-4.2	0.5	102.0	3.0	1.5
-52.4	183	6.3	0.8	-266.1	2.5	1.3
-52.2	189	0.4	0.8	-236.9	3.2	0.4
-51.5	475	38.2	0.2	40.3	0.7	1.5
-50.8	346	38.2	0.4	41.7	1.1	1.1
-50.7	137	5.5	0.8	-257.4	1.6	0.8
-50.3	120	-5.7	0.2	-259.2	0.7	1.1
-49.8	423	-4.3	0.1	103.0	1.0	1.3
-48.8	501	-4.3	0.1	103.7	0.2	2.5
-47.6	9	0.6	1.7	-260.9	3.3	0.4
-46.9	37	-16.3	0.8	58.1	2.0	0.6
-46.2	120	-413.6	0.8	103.6	6.2	1.9
-45.5	57	-10.0	0.7	51.9	1.7	1.3
-44.5	39	8.8	0.2	-281.5	1.0	1.3
-44.4	154	-9.4	0.1	52.8	0.9	1.7
-43.9	29	67.7	0.4	-153.3	1.5	0.8
-42.7	69	67.1	1.0	-54.7	2.6	0.6
-42.4	60	56.3	0.3	-156.6	1.4	1.5
-42.3	44	19.7	1.0	-55.2	2.7	1.5
-42.2	75	-8.5	0.2	56.8	2.2	1.5
-41.9	68	-8.9	0.3	55.6	0.5	1.1
-41.7	110	-445.2	0.5	60.4	2.1	1.1
-41.6	23	56.4	0.4	-154.6	3.0	1.1
-40.2	87	-9.2	0.2	50.2	0.8	1.3
-40.0	67	315.9	0.5	-224.0	3.5	0.6
-39.8	90	55.8	0.3	-154.2	1.1	2.1
-39.2	41	315.3	3.5	-228.7	5.2	0.4
-38.5	41	-3.9	0.3	-280.7	2.2	1.7
-37.4	51	293.7	1.3	-189.1	5.2	0.8
-36.8	63	401.4	1.1	-138.8	2.0	1.5
-36.2	16	29.2	1.4	-62.9	3.0	0.6
-36.0	25	-1.2	1.1	-256.2	2.1	2.5
-35.2	14	34.8	2.9	37.6	2.7	0.8
-34.9	11	28.3	1.3	-257.5	2.7	0.6
-34.5	22	-24.0	3.8	172.1	5.0	0.6
-33.8	196	36.3	0.1	-34.0	0.4	2.1
-33.3	11	119.5	1.5	228.8	7.7	0.4
-31.5	171	-430.7	0.2	71.6	0.7	1.9
-29.9	736	38.4	+-0.1	-175.5	+-0.1	3.2
-28.6	31	-183.6	0.7	-628.3	2.1	0.6
-28.6	151	38.6	0.2	-174.7	0.9	2.1
-28.0	355	-10.4	0.2	31.3	1.5	1.9
-27.4	223	-8.5	0.1	42.4	0.7	1.3
-26.3	50	-185.6	0.3	-619.9	1.2	2.1
-26.1	48	-0.7	0.2	-281.7	1.1	1.1
-25.9	40	35.1	0.5	42.9	1.6	0.6
-24.8	731	2.4	0.2	-280.1	0.4	2.5
-23.0	164	31.2	0.2	15.9	0.8	1.1
-22.7	144	3.1	0.4	-280.7	0.9	0.9
-22.5	74	31.7	0.4	11.2	0.9	1.1
-21.8	152	2.9	0.1	-280.3	0.6	1.5
-20.6	64	35.4	0.4	-2.5	0.8	1.7
-20.5	31	-4.5	0.5	-309.1	4.5	0.8
-20.3	13	136.9	1.7	309.6	6.3	0.6
-19.4	11	-0.8	1.1	123.6	2.8	0.4
-19.4	73	-3.0	0.2	-279.1	0.6	1.3
-19.0	10	-5.8	0.7	124.2	1.8	0.8
-18.6	12	48.0	1.1	-170.8	2.9	0.2
-17.8	9	148.0	1.0	351.6	2.5	0.2
-17.8	9	21.4	2.8	3.5	7.0	0.2
-17.3	45	6.9	1.7	-285.3	2.4	2.3
-16.8	91	50.7	0.3	-160.7	1.7	1.7
-16.1	21	134.2	0.6	310.1	2.7	1.1
-16.1	23	-0.2	1.9	-281.0	1.2	0.8
-15.9	15	-71.0	0.5	202.4	2.0	0.8
-14.6	286	18.2	0.1	10.2	0.5	2.7
-13.6	32	31.9	0.5	23.7	1.8	0.4
-12.9	35	54.6	0.7	-189.7	3.3	1.5
-12.9	18	28.4	1.0	15.0	1.4	0.4
-12.3	46	-417.6	0.5	114.9	2.3	0.8
-12.3	29	20.1	0.9	14.7	3.3	0.6
-11.8	95	-0.6	0.5	-283.1	1.7	3.4
-11.7	44	33.1	0.7	7.5	4.6	0.6
-11.4	43	33.1	1.1	19.4	2.3	1.3
-10.6	58	224.7	0.4	203.9	2.2	1.1
-10.6	115	-3.5	0.2	-283.1	1.0	1.1
-10.2	42	28.0	1.3	27.1	7.9	0.6
-10.1	139	-447.6	0.4	51.8	2.4	1.1
-9.5	199	62.4	0.4	-158.3	2.4	2.7
-8.7	31	144.4	0.3	-299.9	5.4	0.6
-8.7	41	2.9	0.6	-296.3	2.2	0.6
-8.5	61	30.7	0.4	29.5	1.5	1.5
-7.4	56	-2.0	0.3	-286.0	1.6	1.1
-7.0	45	237.1	0.4	-414.0	1.6	2.1
-7.0	59	26.5	1.0	21.7	1.0	1.3
-6.3	330	-447.3	0.2	53.0	0.7	0.8
-6.2	94	19.3	0.6	13.2	1.4	0.4
-6.1	71	-1.8	0.5	-284.7	0.9	1.7
-5.1	727	27.9	0.5	23.4	1.0	1.1
-4.7	744	18.2	1.2	11.5	2.2	2.1
-3.9	50	3.8	0.4	-287.3	1.3	1.1
-2.9	533	591.5	0.1	-57.2	1.4	1.7
-2.8	48	3.1	0.6	-285.5	1.8	0.4
-2.4	72	45.1	0.5	-171.1	3.6	0.4
-2.4	210	28.5	0.3	23.3	0.7	1.1
-2.0	602	556.3	0.3	-102.8	0.9	0.8
-1.5	138	60.4	0.4	-132.9	2.2	0.4
-1.3	1045	556.9	0.2	-102.2	1.8	0.8
-0.8	325	17.6	0.3	3.1	0.7	1.3
-0.7	807	-2.6	0.7	-282.6	2.0	2.3
-0.1	40	228.4	0.5	-421.3	2.2	0.4
0.4	412	59.6	0.3	-137.0	1.3	2.9
0.7	950	17.0	0.3	6.4	0.9	1.7

TABLE 1—*Continued*

VELOCITY KM S^{-1}	FLUX JY	RA OFFSET 0^{m}.001		DEC OFFSET 0^{m}.001		RANGE KM S^{-1}
1.3	53	166.3	+-0.6	343.2	+-2.1	1.1
2.0	175	655.7	1.5	280.3	6.6	0.8
2.1	66	-105.7	0.3	-414.4	1.6	1.3
2.7	63	59.5	0.2	-129.1	1.3	0.6
2.8	203	48.4	0.3	299.1	0.8	1.5
2.9	75	14.7	1.6	-96.4	4.6	0.4
3.1	104	27.7	0.4	-113.0	2.7	0.6
4.1	1097	-506.8	0.1	-9.3	0.5	2.2
4.4	103	29.7	0.8	-126.5	3.2	1.1
4.5	881	606.8	0.4	-1990.7	0.8	1.5
4.7	285	1168.3	2.4	245.4	16.9	0.2
5.1	160	27.0	0.3	-197.1	2.4	0.8
5.3	510	-12.9	0.1	272.0	0.4	1.8
5.9	109	-0.1	0.4	-211.7	1.3	0.9
5.9	120	863.8	0.5	369.8	1.9	0.2
6.1	98	124.0	1.5	2011.5	8.5	0.4
6.4	169	917.4	0.4	321.3	8.2	0.4
6.7	185	239.1	0.3	48.4	1.5	1.7
7.0	300	-10.0	0.2	-41.0	0.9	1.1
7.0	302	942.5	0.4	321.4	6.7	0.8
7.2	1166	-506.1	0.8	-8.4	1.7	1.1
7.2	1119	606.2	0.2	-1990.8	0.7	1.1
7.8	1241	812.3	0.9	462.7	6.7	0.6
8.3	1820	23.8	0.6	-114.4	1.2	1.5
8.5	695	-2.1	0.8	-279.2	1.2	1.3
9.8	1370	14.1	0.3	-212.8	1.2	1.7
9.9	288	3.2	0.3	4.4	1.2	0.6
10.7	4495	1125.2	0.7	290.6	1.7	3.6
10.9	9515	1.6	0.1	3.3	0.2	1.3
11.4	3437	0.0	0.0	0.0	0.2	0.6
12.3	251	7.5	0.3	4.3	0.9	0.9
12.9	2571	556.1	0.2	-98.1	0.5	1.9
13.6	409	713.3	0.5	312.8	2.4	1.1
14.6	162	48.3	0.6	-215.2	1.1	1.5
14.8	1524	1123.9	0.3	288.6	1.2	2.5
16.3	520	1127.7	1.0	288.3	1.8	1.1
16.3	436	712.5	0.8	312.4	1.6	1.1
16.5	719	1075.8	1.1	73.8	3.8	1.9
17.1	317	1115.0	1.0	285.3	2.6	0.6
17.1	68	118.0	0.3	249.0	0.8	0.8
18.0	491	616.4	0.4	355.9	2.1	1.7
18.1	548	1118.1	2.4	285.3	2.4	2.5
18.5	141	712.4	1.1	-1545.1	2.7	0.6
18.8	138	793.4	3.9	976.7	2.0	0.6
19.8	35	59.9	0.3	-96.8	1.5	0.6
20.0	55	980.2	0.5	204.6	1.5	0.4
20.5	122	722.2	0.8	919.2	3.7	1.7
20.7	509	1113.0	0.3	281.6	0.6	1.5
21.5	46	704.2	4.4	-1527.7	23.7	0.4
21.7	40	735.3	3.2	945.0	11.2	0.4
22.0	119	1162.9	1.7	257.0	3.0	0.9
22.4	118	719.4	0.3	319.3	2.4	0.8
22.4	25	492.4	1.0	-1738.7	3.4	0.4
24.3	144	591.4	0.6	385.7	1.1	0.8
24.5	582	1154.7	0.6	192.0	1.3	4.4
27.2	125	1155.2	0.4	192.9	0.6	1.1
28.1	49	493.8	1.9	-1749.0	5.8	0.9
28.4	99	1153.6	1.5	196.1	1.4	1.1
29.7	128	892.2	0.5	16.5	1.2	0.8
30.0	557	1154.0	0.2	193.3	0.9	2.6
32.9	400	1154.3	0.1	195.6	0.6	1.7
33.4	27	927.7	1.3	204.0	4.6	0.2
34.2	732	1154.4	0.1	196.3	0.4	2.5
36.4	205	927.8	+-0.5	204.2	+-1.0	2.5
37.2	23	1175.3	1.8	195.3	4.9	0.8
38.0	41	982.0	0.4	280.0	3.2	1.1
38.7	29	783.6	1.3	298.6	5.5	0.6
39.5	106	1163.8	0.4	187.3	1.7	1.9
40.4	196	1165.4	0.7	238.1	2.4	1.1
41.5	797	628.3	0.1	-1493.2	0.4	3.6
42.5	69	1178.0	0.8	213.0	3.9	1.1
43.7	14	835.4	0.8	974.6	3.2	0.8
44.0	18	918.9	3.4	209.2	9.0	1.1
45.9	16	650.4	2.2	-1463.4	4.8	1.1
46.5	16	1151.7	3.2	199.1	8.8	1.3
47.1	31	628.7	1.0	-1493.7	2.9	1.7
48.2	42	1150.9	3.4	201.7	8.6	2.5
48.3	45	540.6	0.3	-180.5	2.5	0.6
49.2	26	928.7	1.4	200.8	5.2	0.8
49.3	63	705.1	1.4	334.9	5.5	1.9
50.7	21	1164.4	0.8	204.5	8.0	1.7
51.1	23	659.8	1.9	-621.0	7.9	1.1
51.3	6	47.4	1.3	-37.4	3.2	0.2
54.0	171	1110.8	0.2	258.8	0.9	1.9
54.5	27	498.3	1.1	-45.5	4.6	0.6
55.1	25	769.3	1.4	306.5	5.5	0.4
55.8	578	1184.6	0.2	229.5	0.9	1.9
57.1	31	926.0	2.5	217.0	2.9	1.3
58.7	16	1178.6	1.8	223.1	3.7	1.7
59.3	17	474.6	1.0	248.4	3.6	0.6
59.9	19	732.3	5.1	1089.1	4.3	0.8
60.1	6	43.8	2.3	-55.4	8.4	0.4
61.1	19	1109.2	3.2	269.6	6.3	0.4
61.4	20	614.5	5.9	-107.5	21.6	0.6
62.0	81	1137.7	0.9	188.1	3.0	1.1
62.9	64	1137.3	1.1	195.5	5.1	1.7
63.3	210	927.0	0.3	215.0	0.8	3.6
64.7	26	325.4	5.6	65.3	22.2	0.6
66.6	23	926.5	1.0	214.9	3.9	1.3
68.1	65	1177.9	0.7	220.2	1.5	3.4
70.0	11	459.9	5.0	127.6	21.9	0.4
71.7	6	490.6	2.3	-55.2	41.3	0.4
72.3	17	309.7	3.6	202.4	13.6	0.6
73.8	27	701.6	2.9	381.8	7.5	0.8
75.1	384	1183.3	0.3	218.9	1.4	6.1
76.9	34	705.3	5.2	381.6	30.7	1.1
79.4	39	1098.9	0.7	120.3	1.7	2.7
81.4	34	1099.7	0.3	124.4	3.6	0.8
134.3	36	1015.6	0.4	270.9	1.4	1.9
136.5	12	1016.8	0.5	266.2	5.2	0.6
137.2	11	1016.5	1.7	275.0	6.8	0.6
139.3	52	1014.3	0.7	268.8	2.3	2.9
140.9	20	1014.5	0.6	271.3	1.9	1.3
141.4	21	1187.0	0.6	240.0	4.9	0.8
142.6	90	1014.9	0.4	269.6	2.4	1.7
145.8	8	1062.4	3.2	205.7	12.1	0.6
147.1	14	1186.1	1.1	235.4	7.1	0.6
149.2	40	1033.6	3.1	182.5	23.1	1.1
149.2	40	1059.0	1.0	184.9	4.2	2.1
150.0	28	1059.6	1.3	186.9	2.6	1.3
152.4	88	1060.5	0.4	185.1	0.5	2.1
153.4	102	1060.5	0.3	184.6	0.5	3.6
165.3	15	684.4	0.5	496.6	1.9	1.1
166.2	11	682.8	0.6	497.1	2.5	0.9
173.3	36	691.3	0.7	505.6	2.1	2.7
179.2	29	760.9	0.6	547.7	1.1	2.5

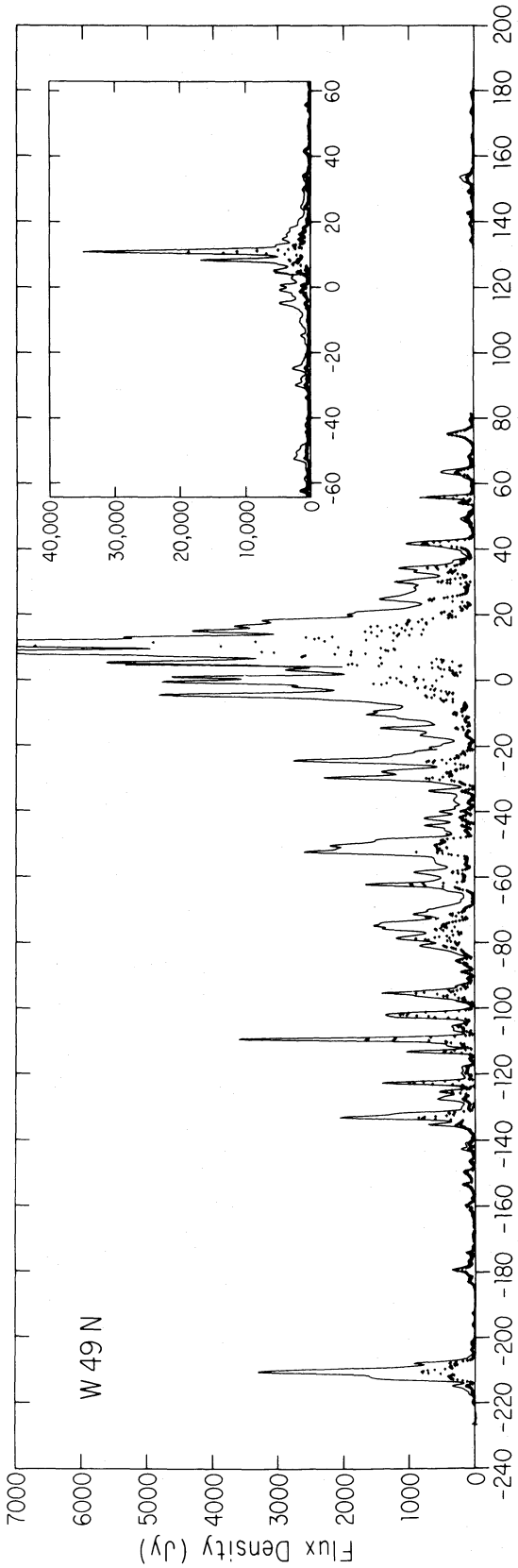

FIG. 2.—The solid line is the total power spectrum of W49N in 1978 June. The symbols show the sum of flux densities in the map points at each velocity. The insert shows the central portion of the spectrum with a ten times larger scale. The flux density scale is uncertain by a large factor as discussed in the text.

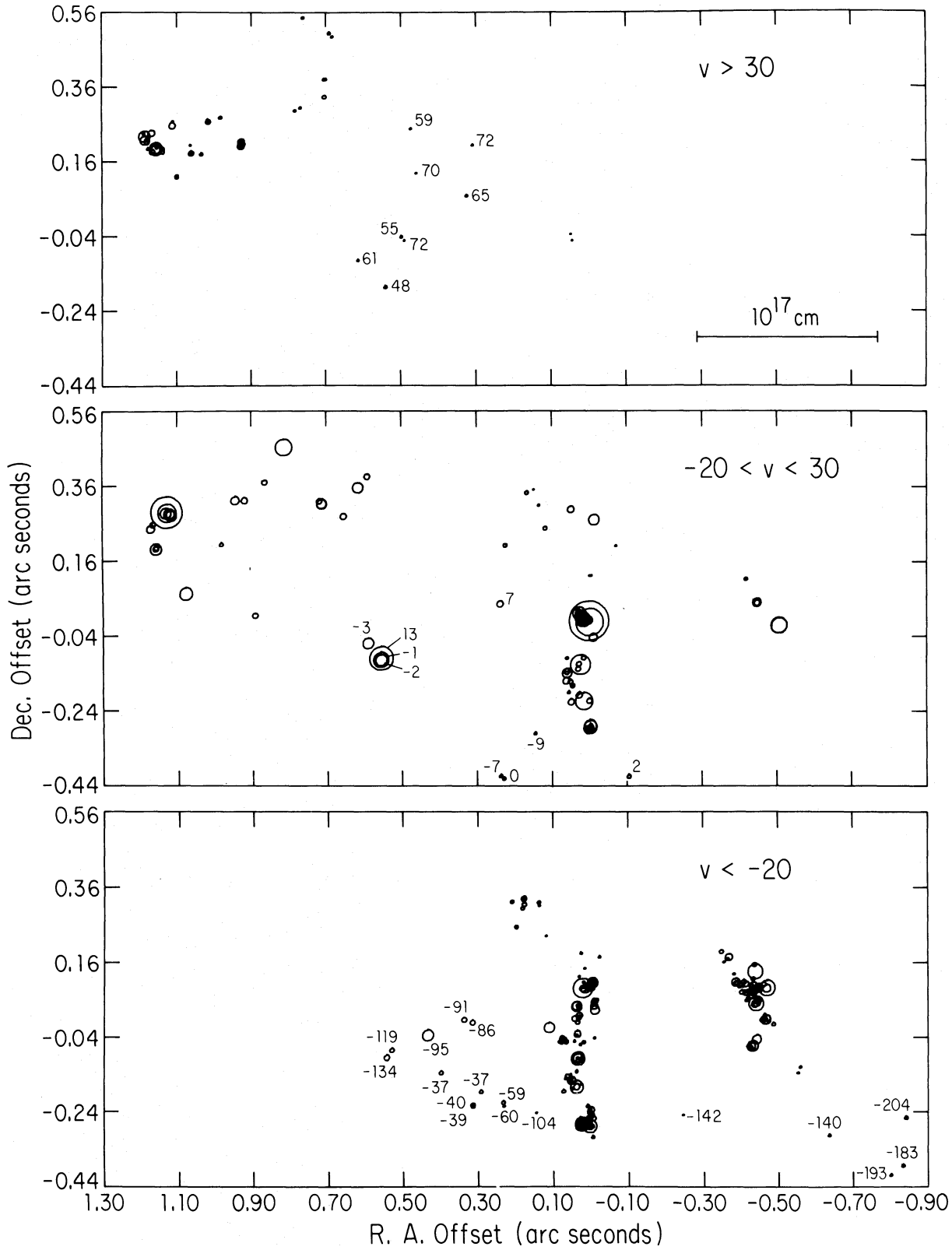

FIG. 3.—These three maps of the same region show the distribution of most of the features in W49 and demonstrate the separation of the positive and negative high velocities. The top map shows positive high velocity ($v > 30$ km s^{-1}) points, the middle map shows the low velocity (-20 km s$^{-1} < v < 30$ km s^{-1}) points, and the bottom map shows the negative high velocity points ($v < -20$ km s^{-1}). The dividing points between high and low velocities are not based on any special observational or theoretical considerations but are merely reasonable values for which the separation of positive and negative high velocity features is clearly demonstrated. The velocities of features not seen in later figures are shown in km s^{-1}.

the maps. Some of the features are probably partially resolved leading to a low cross-correlated flux density. This is the most likely explanation for the missing flux density in some of the apparently isolated high-velocity lines. There are also features which were not mapped due to their low flux density levels compared to other features at the same velocity. This is almost certainly true in the low-velocity regime where there are likely to be a large number of features at each velocity. Such confusion provides motivation for future experiments designed to use the aperture synthesis technique.

Figure 3 demonstrates one of the principal results of the experiment—the pronounced separation of the positive and negative high velocity features. This apparent separation was noted by Walker *et al.* (1977) but was very insecure as it was based on only one VLB map point and one Berkeley interferometer point at high positive velocity. The top map of Figure 3 shows the positive high velocity (velocity greater than 30 km s^{-1}) features in the central region of the full map. The middle map shows the low velocity (velocity between -20 and 30 km s^{-1}) features in the same region. Note that if there are any high velocity features moving in a transverse direction, they will appear here. The bottom map shows the high negative velocity (velocity less than -20 km s^{-1}) features. The spatial separation of the positive and negative high velocity features is clear.

The regions covered by the small scale maps are shown as boxes in Figure 4. Figures 5, 6, 8, and 9 are small-scale maps of particularly interesting regions of the full map. Figures 5 and 6 contain inserts with even smaller scale blowups of regions marked with boxes. Each of the features in the map represents the peak amplitude, velocity of the peak amplitude, and mean position (weighted by the errors) of several map points from different velocity channels. The individual map points can be used to derive spectra of all of the mapped emission in specific regions. Figures 7 and 10 present a number of such spectra corresponding to regions marked with boxes in Figures 5, 6, and 9.

IV. DISCUSSION

The distribution of features in the map of W49N does not clearly reveal the three-dimensional geometry of the maser region. However, it does provide clues to the nature of that region. The separation of the positive and negative high-velocity features and the presence of many isolated features suggest that the whole region is excited by a single source rather than by several separate sources. The clustering of high- and low-velocity features suggests that the masers are occurring where clouds of very different velocities are interacting. The overall distribution shows patterns that would be expected if the masers lie in shell-like structures. These clues are discussed in detail below, and a possible geometry of the maser region is presented at the end of this section. A statistical analysis of the distribution of features will be presented in a future paper.

The separation of the positive and negative high-velocity features is one of the most striking features of the map. The map contains 67 features with velocity greater than 30 km s^{-1} and 211 features with velocity less than -20 km s^{-1}, so the separation is now well established. The regions of positive and negative high-velocity features overlap slightly. However, they are probably completely separated, and the small overlap is a projection effect.

The separation can be explained if the dynamics of the whole region are determined by a central exciting source or if there are several exciting sources and there is some mechanism which favors high velocity masers of one sign or the other around each source. In either case, the exciting sources are probably newly formed OB stars (cf. Genzel *et al.* 1978). In the first explanation, a central star is blowing material away from itself. The high-velocity maser emission may occur at the boundary where this material encounters a surrounding molecular cloud, or it may occur in dense blobs of gas driven from near the star. The separation is explained by an offset in the line of sight to the Earth between the regions of maser emission on the near and far sides of the central source. Systematic outflow over a region of similar size has been observed in Orion-KL (Genzel *et al.* 1981*a*). In the second explanation, a number of stars might, for example, exist inside a bubble in a molecular cloud. The bubble could be the H II region formed by the group of stars. Each star excites maser emission on the boundary of the H II region where that boundary is close to the star. The high velocity

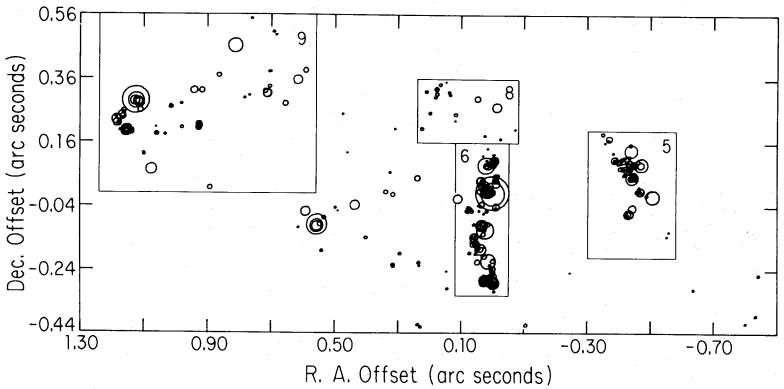

FIG. 4.—A map of all of the features in Fig. 3 showing the regions that are expanded in Figs. 5, 6, 8, and 9

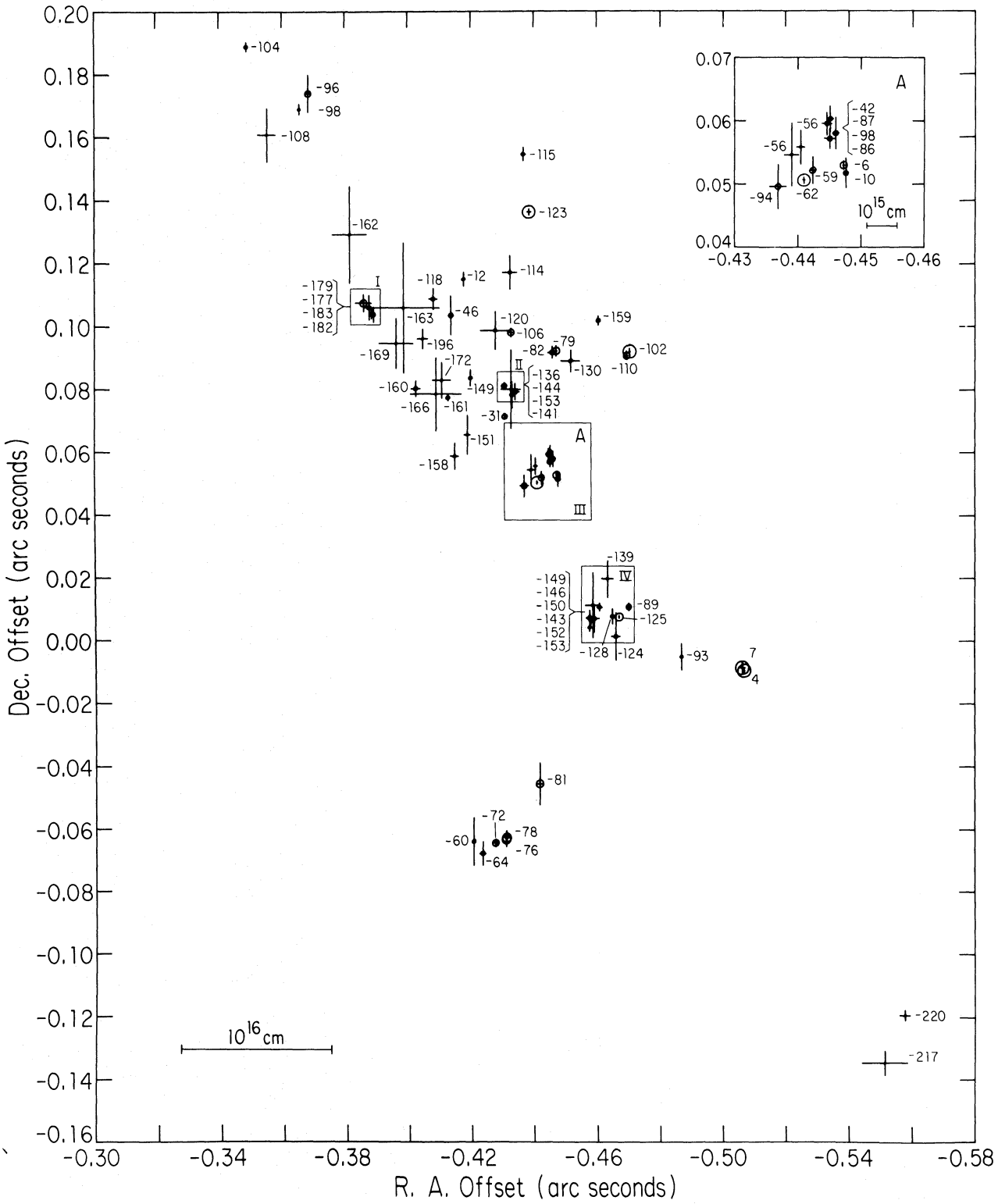

FIG. 5.—An expanded map of the western cluster of features. The insert shows an even further expanded view of the region of the box marked with an A. The boxes marked with Roman numerals show the regions for which spectra are given in Fig. 7. In all of the small scale maps, each feature is marked by a circle whose area is proportional to its flux density and by a cross whose arms represent the one sigma positional error bars.

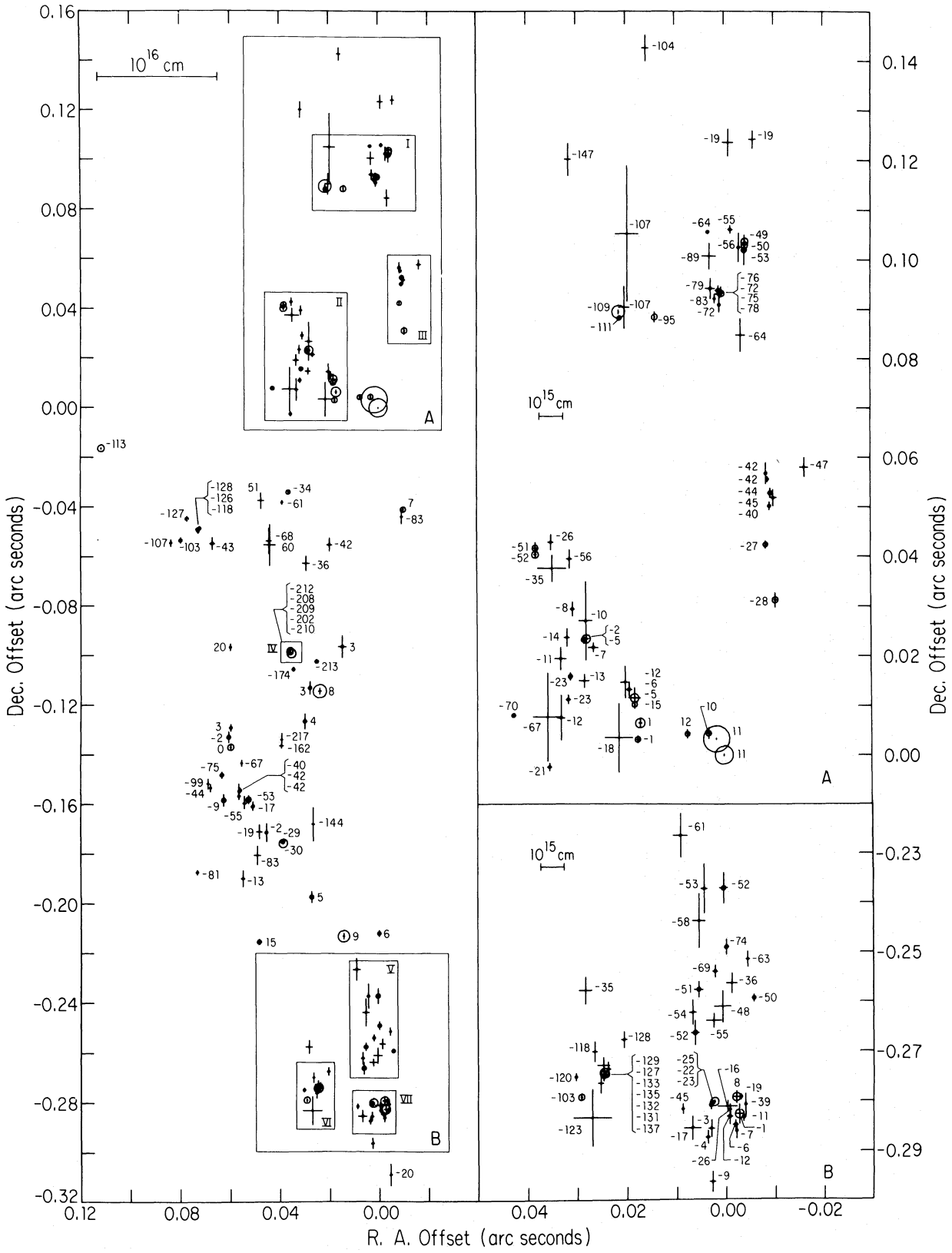

FIG. 6.—Expanded views of the main north-south cluster of features. The left map shows the whole region as marked in Fig. 4. The two right maps show further expanded views of the regions marked A and B. The boxes marked with Roman numerals show regions for which spectra are presented in Fig. 7.

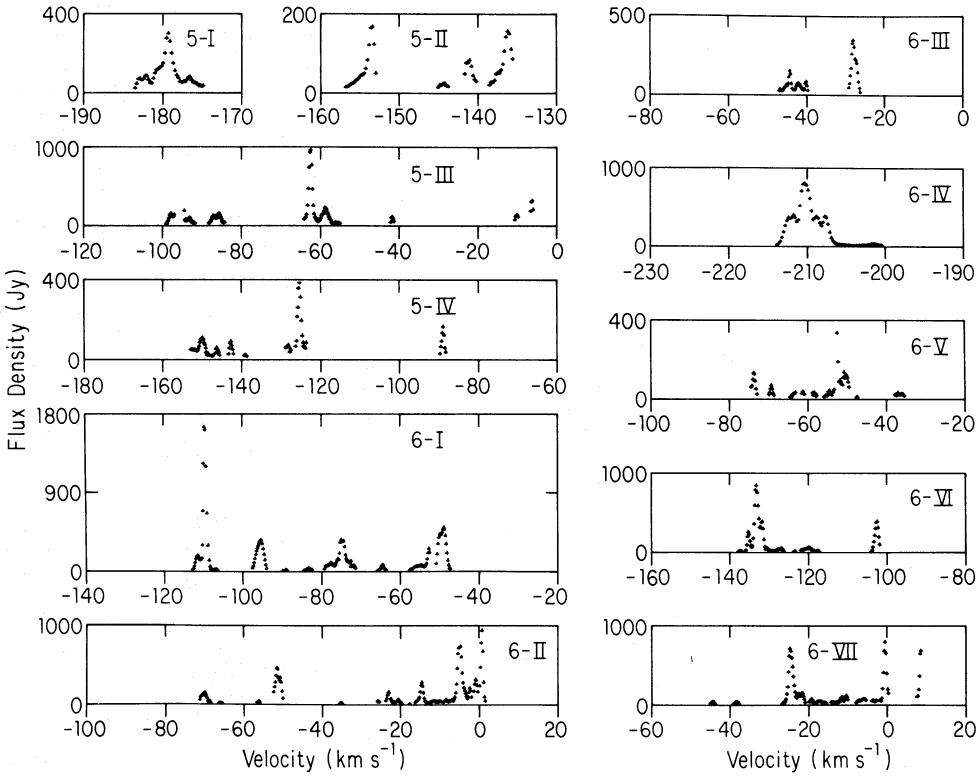

FIG. 7.—Spectra of selected regions marked by boxes in Figs. 5 and 6. The spectra represent the sum of the flux densities at each velocity of all features whose mean position falls within the box.

features occur at the boundary in material that is driven away from the star. The separation would be a result of stars on the near side of the bubble being along a different line of sight from those on the far side.

Walker *et al.* (1977) found that the masers in W49N are clustered in several centers of activity. This clustering has been used as evidence that there are several sources of excitation. The current map shows that, while most features are still found in clusters, there are a large number of isolated features as well. The fact that these isolated features include high velocity features runs counter to another observation of Walker *et al.* (1977)—that there is a close association of high- and low-velocity features. Again, the earlier observation is true for most features, but with the very large number of features in the new map, it is seen to break down in a significant number

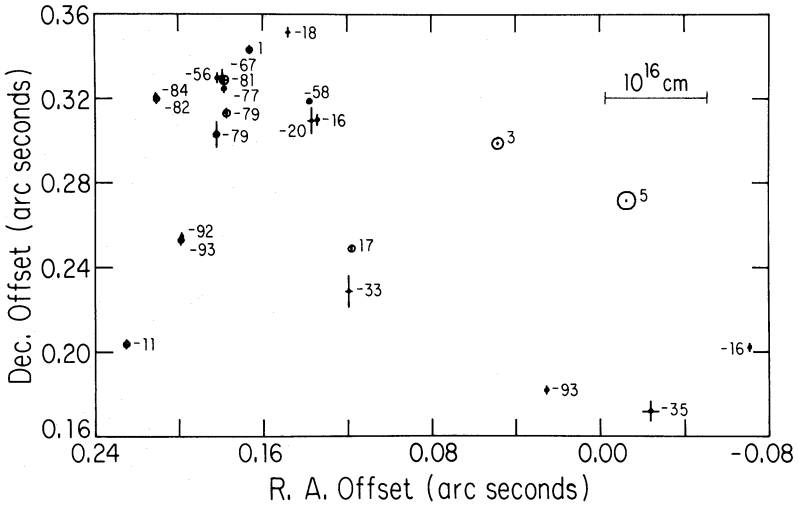

FIG. 8.—Small-scale map of the region shown by the box marked 8 in Fig. 4

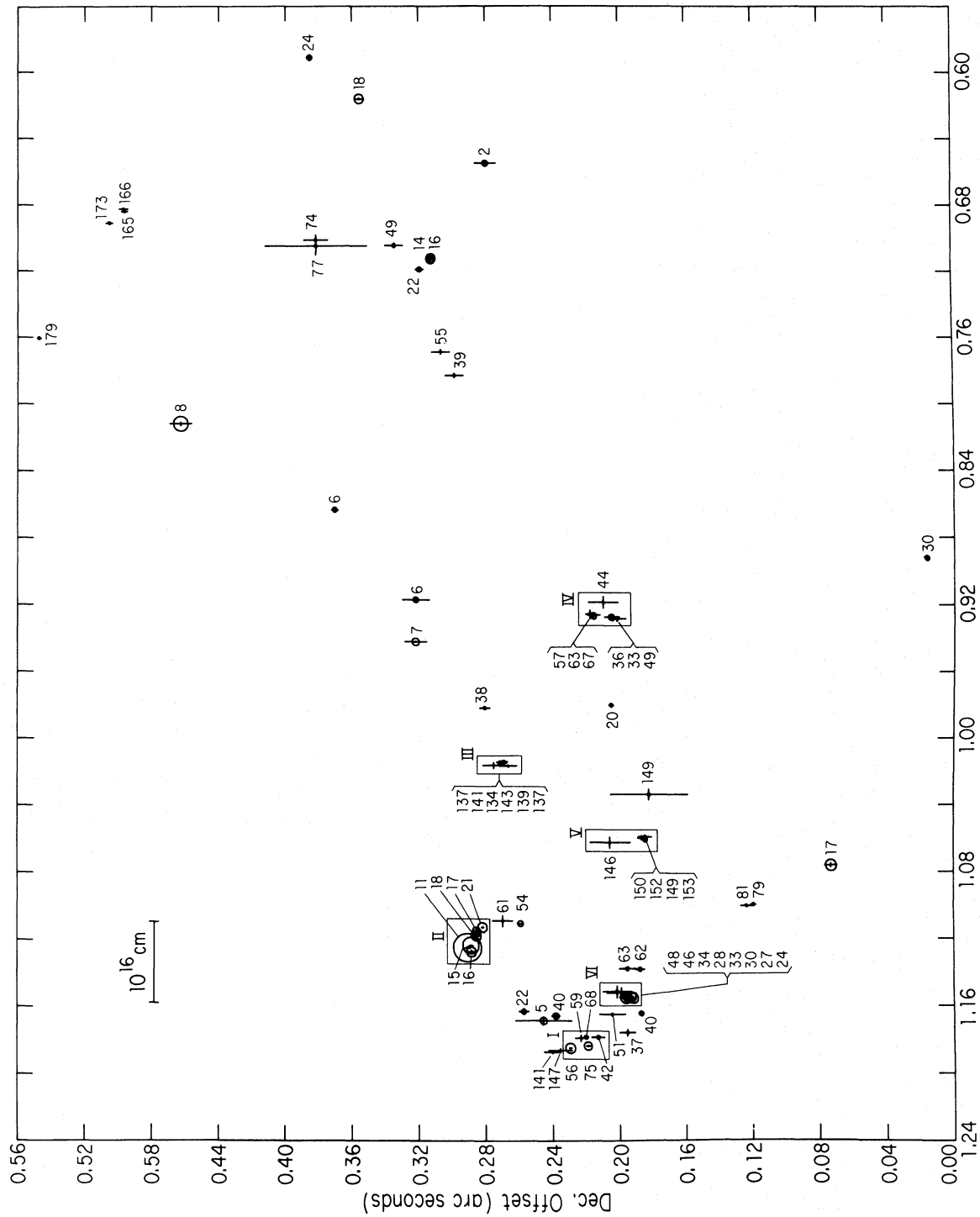

FIG. 9.—Small-scale map of the eastern clusters of features. Boxes marked with Roman numerals show regions for which spectra are presented in Fig. 10.

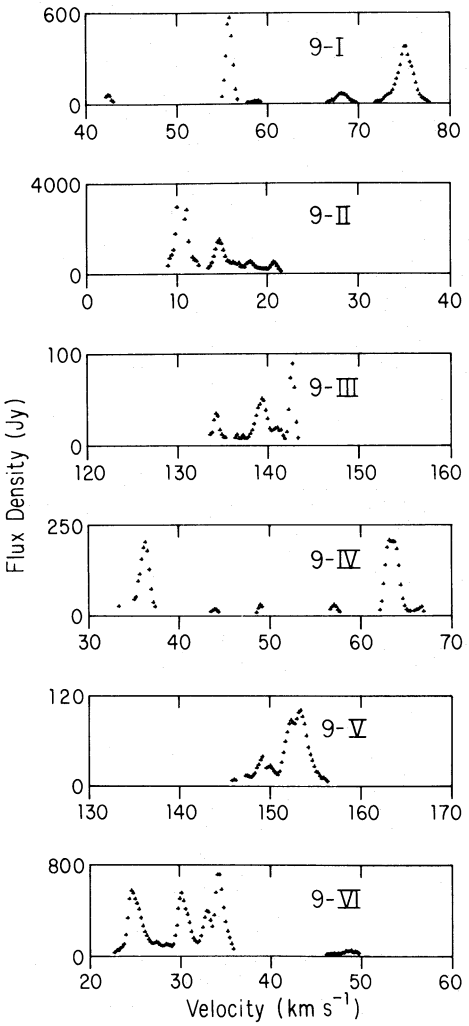

FIG. 10.—Spectra of regions marked by boxes in Fig. 9

of cases. Unless we postulate the existence of a very large number of exciting stars, the isolated features show that maser emission can occur at distances greater than 10^{17} cm from the source of excitation. Given that this is possible, one of the objections to a single source of excitation, that the masers are too far from the energy source, must be reexamined. While the evidence is certainly not conclusive, the least complex explanation for the data is that there is a single source of excitation in the W49N maser region.

The relative distributions of the isolated features and the major clusters show patterns that suggest that the masers lie on shell-like structures. If the masers were distributed on the surface of a shell, concentrations of features would be expected where the shell is seen edge-on due to projection effects. These concentrations would separate face-on regions of the shell where relatively isolated features would be seen from regions outside the shell which would be devoid of features. The clearest cases of this type of structure are seen at the eastern end of the maser region and in the vicinity of the reference position. However, the shapes of the concentrations and the presence of both isolated features and a large cluster west of the reference position show that, if the masers do lie on a shell, that shell must have a complex geometry. The roughly circular, 0".4 hole in the distribution of masers west of the reference position is also suggestive of a shell, although it would have reversed inner and outer regions from the shell implied by the isolated features. A close examination of the distribution of velocities within the major concentrations of features forming this "shell" provides no evidence for the circular symmetry that might be expected in a shell. In fact the three major clusters of features involved (Fig. 5 and Fig. 6, inserts A and B) appear rather similar and show velocity gradients to the north and east. The implications of these similarities are not clear, but they may be evidence that the kinematics are controlled by factors operating over a larger region than the 0".4 hole.

There are many regions in the map where a wide range of velocities is seen in a very small area. A striking example is seen in spectrum 6-IV of Figure 7 which shows emission over a velocity range of almost 15 km s^{-1}, centered at -208 km s^{-1}, all of which is located at the same spot to within the positional errors. Since the hyperfine lines only cover a range of 5.8 km s^{-1}, the major fraction of this spread must be due to kinematic effects (Nonkinematic explanations for high velocity masers seem to be excluded by the observations of proper motions in Orion and W51 by Genzel *et al.* 1981*a*, Genzel *et al.* 1981*b*, and Schneps *et al.* 1981.) It is as though we are looking down the length of an accelerating or decelerating streamer. Note that these kinematic effects probably do not control the maser variations since, at 15 km s^{-1}, about 10 years are required to traverse a typical maser cloud (5×10^{14} cm—see Walker *et al.* 1978), while a typical time scale for variations is several months. Wide velocity ranges are also seen in the form of broad line widths for a number of individual features. These broad lines again suggest that we are seeing velocity gradients along the line of sight. In general, the wide features tend to be high-velocity features, but this may be a selection effect because the high-velocity features tend to be isolated and easy to observe. The broad wings of a wide low-velocity feature are liable to be swamped by other features at similar velocities. However, a similar correlation between line width and velocity has been noted by Genzel *et al.* (1981*a*) for three other maser regions. On a larger scale than individual features, the clusters show the close association of features over wide ranges of velocity. Possible implications of this association are discussed below.

Maser theory and observations have recently been reviewed by Reid and Moran (1981). Water masers such as those in W49N are thought to occur in the vicinity of newly formed, massive stars. The emitting regions have temperatures of about 300–1000 K and H_2 number densities of 10^7–10^{11} cm^{-3}. These conditions might exist in disks (cf. Elmegreen and Morris 1979) or shells (cf. Genzel *et al.* 1978; Elitzur and de Jong 1978; Norman and Silk 1979) around newly ignited OB stars. The high-velocity

features may be from fragments of the disk or shell driven away from the star by a stellar wind or by radiation pressure (Strelnitskii and Syunyaev 1973). Our observations do not clearly support or reject any of these models. A disk model such as that of Elmegreen and Morris probably requires several disk systems to explain the distribution of low velocity emission which leaves the origin of the separation of positive and negative high velocity emission in question. On the other hand, calculations of shell parameters (Cochran and Ostriker 1977; Yorke and Krugel 1977) show that there are problems producing the required maser temperatures and densities at distances of more than 10^{16} cm from the exciting star (Walker *et al.* 1978).

Our observations, together with a general constraint on the acceleration of high velocity maser cloudlets, suggest a possible geometry for the W49N maser region. As discussed above, the distribution of high velocity features is most easily explained if the whole region is excited by a single star. The clustering of features with large velocity differences shows that these features are related and suggests that either acceleration is occurring within the clusters or the cluster mark regions of interaction between clouds with different velocities. If the high velocity masers are accelerated by a stellar wind or by radiation pressure from the central star, the acceleration probably is not occurring in the clusters. Strelnitskii and Syunyaev (1973) have shown that the acceleration must begin much closer to the star than 10^{16} cm for reasonable maser and stellar parameters, but the clusters are separated by distances of more than 10^{17} cm. Therefore, the clusters are probably regions of interaction, perhaps on a shell around the central star, where high velocity material which was accelerated close to the star, is impinging on slower material or the surrounding molecular cloud. The concept that masers occur where high velocity clouds are being decelerated has been used by Elmegreen and Morris (1979) to explain remote, high-velocity features, and they show that conditions can be appropriate for masers in such regions. The interaction helps compress the clouds to maser densities and may help provide conditions appropriate for a collisional pump. In this scenario, the large velocity ranges seen in clusters are the result of the mixing and deceleration occurring in the interaction regions. Isolated features may mark interaction regions where the maser conditions are marginal and only one maser appears. The high-velocity material may originate in a disk or fragmenting shell near the central star. There is no obvious evidence in our map to indicate the location of the star.

We wish to thank C. Spencer, H. Hardebeck, and F. Isreal for their efforts in installing a University of California, Berkeley maser on the Owens Valley Telescope, and we thank A. Cheung for allowing the use of that maser. We also thank B. Allen, B. Burke, J. Moran, and S. Lichten for assistance during the observations. R. C. W. gratefully acknowledges the support of the Owens Valley Radio Observatory during much of this work. The work of J. A. G.-B was supported in part by the Consejo Nacional de Ciencia y Tecnología, México. VLBI research at the Owens Valley Radio Observatory and at the Haystack Observatory is supported by the National Science Foundation. Part of the work done at the RLE, M.I.T. is supported by the National Science Foundation.

REFERENCES

Clark, B. G. 1973, *Proc. IEEE*, **61**, 1242.
Cochran, W. D., and Ostriker, J. P. 1977, *Ap. J.*, **211**, 392.
Elitzur, M., and de Jong, T. 1978, *Astr. Ap.*, **67**, 323.
Elmegreen, B. G., and Morris, M. 1979, *Ap. J.*, **229**, 593.
Genzel, R., *et al.* 1978, *Astr. Ap.*, **66**, 13.
Genzel, R., *et al.*, 1981*a*, *Ap. J.*, **247**, 1039.
Genzel, R., Reid, M. J., Moran, J. M., and Downes, D. 1981*b*, *Ap. J.*, **244**, 884.
Giuffrida, T. S. 1977, Ph.D. thesis, Massachusetts Institute of Technology.
Knowles, S. H., Johnston, K. J., Moran, J. M., Burke, B. F., Lo, K. Y., and Papadopoulos, G. D. 1974, *A.J.*, **79**, 925.
Norman, C. A., and Silk, J. 1979, *Ap. J.*, **228**, 197.
Reid, M. J., Haschick, A. D., Burke, B. F., Moran, J. M., Johnston, K. J., and Swenson, G. W. 1980, *Ap. J.*, **239**, 89.
Reid, M. J., and Moran, J. M. 1981, *Ann. Rev. Astr. Ap.*, in press.
Schneps, M., Lane, A. P., Downes, D., Moran, J. M., Genzel, R., and Reid, M. J. 1981, *Ap. J.*, **249**, 124.
Strelnitskii, V. S., and Syunayaev, R. A. 1973, *Soviet Astr.—AJ*, **16**, 579.
Walker, R. C., Johnston, K. J., Burke, B. F., and Spencer, J. H. 1977, *Ap. J.* (*Letters*), **211**, L135.
Walker, R. C. 1981, *A.J.*, **248**, 256.
Walker, R. C., *et al.* 1978, *Ap. J.*, **226**, 95.
Wilson, T. L. 1975, in *Lecture Notes in Physics*, Vol. **42**, H II *Regions and Related Topics*, ed. T. L. Wilson and D. Downes (Berlin: Springer-Verlag), p. 424.
Yorke, H. W., and Krugel, E. 1977, *Astr. Ap.*, **54**, 183.

J. A. GARCIA-BARRETO: Research Laboratory of Electronics, Massachusetts Institute of Technology, Building 26-355, Cambridge, MA 02139

D. N. MATSAKIS: U.S. Naval Observatory, 34th and Massachusetts Avenue, N.W., Washington, DC 20390

R. C. WALKER: National Radio Astronomy Observatory, Edgemont Road, Charlottesville, VA 22901